Materials Advances

ROYAL SOCIETY OF CHEMISTRY

PAPER

View Article Online
View Journal | View Issue

Cite this: *Mater. Adv.*, 2023, 4, 2384

Synthesis and characterization of nano-crystallite triple superphosphate from waste *Pila globosa* shells for sustainable industrial production†

Md. Sahadat Hossain, [a] Md. Aftab Ali Shaikh,*[ab] Md. Farid Ahmed[a] and Samina Ahmed *[ac]

The purpose of this research work was to explore the sustainable industrial application of waste *Pila globosa* (*P. globosa*) shells, commonly known as apple snail shells, *via* synthesizing nano triple superphosphate [TSP, $Ca(H_2PO_4)_2{\cdot}H_2O$]. An exothermic reaction between *P. globosa* shells and phosphoric acid, which were the precursors of calcium and phosphate respectively, facilitated the production of TSP. The synthesized TSP was characterized by using thermogravimetric analysis (TGA), differential scanning calorimetry (DSC), X-ray diffraction (XRD), Fourier transform infrared (FT-IR) and Raman spectroscopies, field emission scanning electron microscopy (FESEM), UV-Vis-NIR spectroscopy, and wavelength-dispersive X-ray fluorescence (WDXRF) spectroscopy. TGA showed promising results by providing the remaining mass (including 2.42% free water) value as 77.63%, which is very close to the theoretical remaining mass percentage (78.57%). Thus, this observation acts as good evidence for the formation of TSP in nearly pure phase. Furthermore, crystallite size was assessed with the aid of different model equations, and a reasonable value of crystallite size was achieved from the Sahadat–Scherrer model (99 nm) and three peaks model (88 nm). The WDXRF analysis of the synthesized TSP showed good evidence that it contained 76.9% of P_2O_5, much higher than the minimum requirement for commercial applications. A fixed amount of water was added to this reaction process to eliminate the drying procedure, which will minimize the production cost but increase the yield. This research revealed that *P. globosa* shells are a potential precursor of calcium as a new raw material source of P-fertilizer and 60% (w/w) phosphoric acid to minimize the production cost by eliminating the extra drying process with 76.9% P_2O_5 content. Hence, *P. globosa* shells will certainly be an alternative source to meet the demands of raw materials to synthesize phosphate-based fertilizers.

Received 3rd March 2023,
Accepted 29th April 2023

DOI: 10.1039/d3ma00102d

rsc.li/materials-advances

Introduction

The world population is increasing day by day and correspondingly the demand for food is augmenting while no expansion but rather a decrease of the land is becoming crucial.[1] Hence, researchers throughout the world have paid attention to greatly increasing food production within the scope of utilizing limited land. To increase food production, application of chemical fertilizers has expanded immensely. Most of the applied fertilizers are nitrogen, phosphorus and sulfur based, which have positive effects in increasing crop production.[2] Phosphate-based fertilizers are produced mainly from rock phosphate minerals, which are becoming scarce.[3,4] Cordell *et al.* in their assessment[3] pointed out that the demand for phosphorus will surpass resources by 2035 and as a consequence mineral phosphorus will disappear. The declining trend of natural resources is the result of several factors, *e.g.* (i) inefficient utilization of resources; (ii) reluctance in finding new and or alternative resources; (iii) no concern about recycling or reuse; and (iv) high price of chemically synthesized products. The demand for P-based fertilizer was 5 Tg per Yr in 1961 and it had increased to 18 Tg per Yr in 2018, and a prediction has been made that this demand will be increased to 22–27 Tg per Yr in 2050.[5] In a report of *Nature Proceedings*, Shekhar *et al.* remarked that approximately 140 million tons of rock phosphates are produced and consumed across the globe, and most of these rock phosphates are utilized in the production of phosphate fertilizers.[6] However, a few countries already disclosed their concern about the scarcity of phosphate rock for the production of P-fertilizer.[7] The diminishing scenario of P-fertilizer was noted as an "impending shortage" in previously published literature.[8] Thus exploring new

[a] *Institute of Glass & Ceramic Research and Testing, Bangladesh Council of Scientific and Industrial Research (BCSIR), Dhaka-1205, Bangladesh. E-mail: shanta_samina@yahoo.com, aftabshaikh@du.ac.bd*
[b] *Department of Chemistry, University of Dhaka, Dhaka-1000, Bangladesh*
[c] *BCSIR Laboratories Dhaka, Bangladesh Council of Scientific and Industrial Research (BCSIR), Dhaka-1205, Bangladesh*

† Electronic supplementary information (ESI) available. See DOI: https://doi.org/10.1039/d3ma00102d

sources of raw materials has become an urgent need for fertilizer industries. Besides finding new sources, proper distribution of the sources is another vital issue which has to be considered, *e.g.* Russia's invasion of Ukraine is causing problems in the global smooth flows of materials.[9]

Certainly, though rock phosphate or phosphorite is being used as a standard source material for the synthesis of P-fertilizer,[10] locating phosphorite concentrates efficiently and sustainably is a major concern of researchers.[10] However, another problem which is associated with the utilization of rock phosphate is its time-consuming reaction. Usually the conventional industrial process to synthesize superphosphate involves the reaction between rock phosphate and sulfuric acid which requires a fairly long time for the completion of the reaction.[11] Moreover, the purity ($\sim$90%) is also creating problems regarding the application of phosphate-based fertilizer as well as relevant industrial efficiency.[12] Accordingly, alternative sources must be explored in this regard.

Indeed, in the 21st century the focus of researchers has furthermore shifted to 'waste-to-wealth' concept aiming to promote a sustainable lifestyle.[13–17] According to the World Bank, worldwide municipal solid waste, which is only a part of bio-waste of urban areas, may rise to 2.2 billion tonnes per annum by 2025, and in developing countries the projection of escalation of waste generation rate over the next two decades is twofold.[17] Concerning the bio-waste disposal problem, utilization and or recycling of bio-waste for sustainable development has now emerged as a thrust area of research and a number of literature reports are available in this regard.[13–17]

Pila globosa (*P. globosa*) or apple snail shells are enriched with calcium carbonate usually ranging from 95 to 99%. Having such a high calcium content, they are being used in different types of industries, including their derivative products (CaO).[18,19] The shells of *P. globosa* are considered as waste materials and researchers are exploring new applications for them. Few researchers have noted the application of *P. globosa* shells in the production of industrial-grade fertilizers. Recently, we have reported the application of *P. globosa* shells in the production of gypsum fertilizer.[20] Following our previous approach, in this research work, we have used *P. globosa* shells as an alternative source of raw material for the production of triple superphosphate (TSP). Moreover, we have also attempted to simplify the reaction procedure, aiming to increase the yield and thus minimize the production cost.

Materials and methods

Materials

Waste *P. globosa* shells were collected from the wetland of Mirzapur Upazila, Tangail district, Bangladesh. The shells were separated from the soft part and dried under sunlight after cleaning with tap water. The cleaned and dried shells contain 97% calcium carbonate as estimated by the WDXRF technique. Concentrated (85%) orthophosphoric acid was received from E-Merck, Germany and used without further purification. Deionized water used in the synthesis process was prepared in the Glass Research Division of the Institute of Glass and Ceramic Research and Testing, BCSIR.

Synthesis of triple superphosphate

A batch mode protocol was adopted to synthesize TSP at a lab scale. At the initial stage of the synthesis procedure a 60% (w/w) solution of orthophosphoric acid was prepared from 85% (w/w) acid using distilled water in a vessel. Waste shells of *P. globosa* were finely ground using a high-speed ball mill (model: Pulverisette 5 classic line planetary ball mill) to increase the surface area for chemical reaction. The acid was then mixed with the powdered snail shell maintaining a powder to acid molar ratio of 1 : 2. The mixture was continuously stirred until the completion of the reaction. Eqn (1) represents the entire synthesis procedure:

$$CaCO_3(P.\ globosa\ \text{powder}) + H_3PO_4 + H_2O \rightarrow Ca(H_2PO_4)_2{\cdot}H_2O + \text{Heat} \quad (1)$$

Here, one mole of water was trapped in the crystals of TSP and the remaining water was removed as a consequence of heat generated during the hydration reaction. No further heating or filtration was adopted in this procedure and within 24 h the sample was completely dried at ambient condition. Synthesized TSP was then stored in a polyethylene bag for further analysis.

A schematic representation of the synthesis procedure is illustrated in Scheme 1 which can also be adopted in the case of preliminary design for a pilot plant study as well as industrial-scale production.

Thermogravimetric analysis (TGA)

The thermal properties of the synthesized products were evaluated by a simultaneous thermal analysis machine (NETZSCH STA 449F5 STA449F5B-0167-M). The range of operating temperature was 27 to 1000 °C while the heating rate was 10 °C min^{-1}. An alumina sampling chamber was utilized and nitrogen gas was purged for an inert atmosphere. TGA and DSC data were recorded from the thermal analysis.

X-ray diffraction analysis

Using a Rigaku Smart Lab XRD machine, crystallographic phase analysis of the prepared products was accomplished.

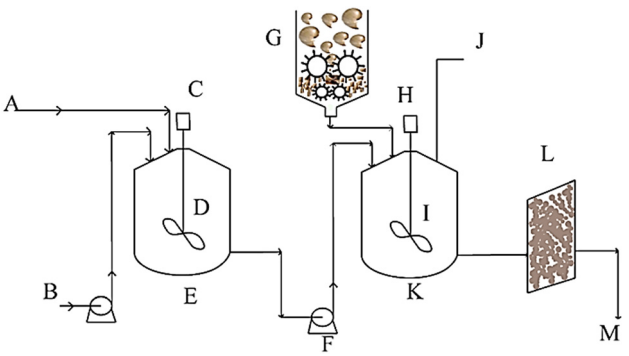

Scheme 1 Process flow diagram for the synthesis of triple superphosphate. Notations: A = 85% H_3PO_4 inlet, B = deionized water inlet pump, C = motor, D = stirrer, E = vessel for acid dilution, F = 60% acid inlet pump, G = ball mill, H = motor, I = stirrer, J = CO_2 vent, K = main reactor, L = drying unit, M = final product.

The data were collected by setting the 2θ range as 5 to 70 degrees maintaining 0.01 steps while the temperature was 23 °C and the cooling-water flow rate was 4.6–4.8 L min^{-1}. The instrument was equipped with a copper tube (CuKα, λ = 1.54060 Å) for the production of X-rays and the operating current and voltage were 50 mA and 40 kV, respectively. Bragg–Brentano parafocusing geometry mode was involved to record the data of the samples as well as for calibration with a standard silicon reference. The phases of the synthesized samples were identified utilizing pdf + 4 2022.

FT-IR spectroscopic analysis

The functional groups of the products were identified using an IR-Prestige 21 machine (Shimadzu, Japan) which was equipped with an attenuated total reflection system. The spectra were recorded from 400 to 4000 cm^{-1} on percentage transmittance basis maintaining 30 scans and 4 cm^{-1} spectral resolution.

Raman spectroscopic analysis

The functional group analysis of TSP samples was conducted using a high-resolution Raman spectrometer (model: HORIBA MacroRAM™ Raman spectrometer) combined with the following features: (i) power 7-450 mW; (ii) wavelength 785 nm; (iii) spectrograph focal length 115 mm; and (iv) spectral range 100–3500 cm^{-1}.

Field emission scanning electron microscopic analysis

The morphological analysis of the synthesized TSP was explored using a field emission scanning electron microscopy (FESEM) instrument (model: JEOL JSM-7610F). The images were captured at an accelerating voltage of 15 kV.

UV/Vis/NIR spectroscopic analysis

To explore the optical bandgap energy, a UV/Vis/NIR spectrophotometer (model: PerkinElmer LAMBDA 1050+) was used. A scan range of 250–800 nm wavelength was maintained. Solid powder samples were used for the measurement of absorbance. The temperature and humidity were 25 °C and 60% respectively during the measurements.

Moisture analysis

The percentage of moisture was determined by following an established method as described in the literature.[21] In short, to determine the moisture content of the synthesized fertilizer, the sample was kept undisturbed in a vacuum oven for 2 h adjusting the temperature and pressure at 50 °C and 500 mmHg respectively. To ensure the accuracy of the data identical analysis was repeated five times and the average data were considered. Furthermore, using a moisture analyzer, moisture content of TSP was also determined at 120 °C.

Results and discussion

Thermal properties analysis

Fig. 1 and 2 exhibit the collected TGA and DSC data of synthesized TSP at various temperatures. The mass loss below

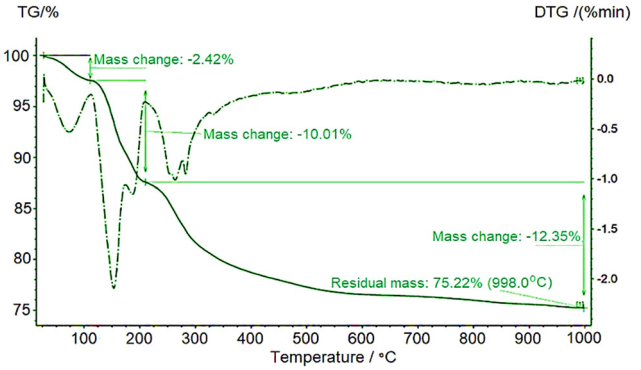

Fig. 1 Thermogravimetric behavior of synthesized TSP.

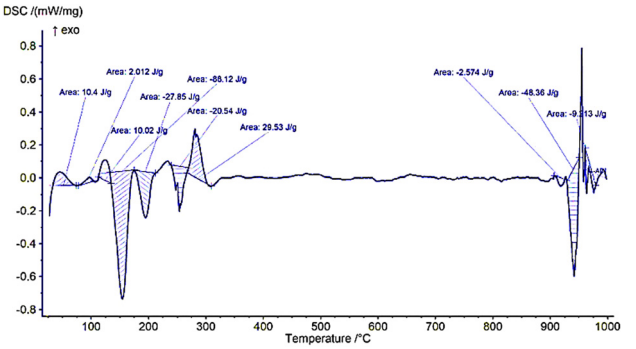

Fig. 2 Differential scanning calorimetry behavior of synthesized triple superphosphate.

100 °C resulted from the removal of the free moisture associated with the sample and nearly 2% of moisture was evaporated at this stage which can be expressed by eqn (2). Next three steps were attributed to three dehydration processes. (i) Dehydration of physisorbed water occurred by removal of one molecule of water from the crystal structure of the TSP. Commencing from 100 °C, this dehydration phenomenon continued up to 200 °C and the associated chemical reaction (*i.e.* formation of anhydrous calcium dihydrogen phosphate) is presented in eqn (3). Due to dehydration, nearly 10% mass loss was noticed and the peak was found at 150 °C in the DTG curve. However, in the DTG curve another tiny peak was visualized at 186 °Cthe intensity of which was very insignificant as compared to the peak observed at 150 °C. The existence of this peak is also allied with the removal of another type of water molecule. (ii) The second dehydration peak as noticed at 250 °C is due to the formation of calcium dihydrogen pyrophosphate and accredited to the loss of one mole of water from orthophosphate. The corresponding reaction is represented in eqn (4). (iii) The third dehydration range was above 350 °C. At this stage, calcium dihydrogen pyrophosphate released one mole of water to form calcium metaphosphate and as a whole nearly 12% mass was lost (eqn (5)). On the other hand, the DTG data also supplemented the maximum amount of mass loss within 400 °C coupled with peak positions at 260 °C and 280 °C. Additionally, remaining negligible mass loss up to 1000 °C was also noticed here.

The DSC plot in Fig. 2 furthermore visualized three endothermic peaks within the region of 320 °C and it has already been revealed from TG/DTG analysis that three types of water were removed within this region. The dehydration reaction is a well-defined endothermic reaction and was reported in connection with many thermal analysis data.[22] The second endothermic peak remained on both sides of 200 °C and comparing with the TG/DTG and DSC figures it can be predicted that this peak was due to the formation of calcium dihydrogen pyrophosphate as expressed in eqn (4). Near 300 °C an exothermic peak was noticed which may be due to the formation of calcium pyrophosphate crystals. Many previous reports have explained crystallization as an exothermic reaction based on DSC analysis.[23] No significant mass loss was recorded after 800 °C in TG/DTG analysis but an exothermic peak accompanied by an endothermic one was visualized in the DSC curve which may result from the phase transformation of β-$Ca(PO_3)_2$ and α-$Ca(PO_3)_2$ (these types of phase transformation were reported at high temperature[24]). From the TG data, about 75.21% mass remained and if the free water percentage (2.42%) is counted the remaining mass is 77.63%. The theoretical remaining mass is 78.57% which was very close to the data of TG. Thus, these data are good evidence for the formation of TSP in nearly pure phase.

$$Ca(H_2PO_4)_2{\cdot}H_2O \text{ with free moisture} \rightarrow Ca(H_2PO_4)_2{\cdot}H_2O + \text{free moisture}\uparrow \quad (2)$$

$$Ca(H_2PO_4)_2{\cdot}H_2O \rightarrow Ca(H_2PO_4)_2{\cdot}H_2O\uparrow \quad (3)$$

$$Ca(H_2PO_4)_2 \rightarrow CaH_2P_2O_7 + H_2O\uparrow \quad (4)$$

$$CaH_2P_2O_7 \rightarrow CaP_2O_6 + H_2O\uparrow \quad (5)$$

Crystallographic analysis

The crystallographic analysis of the product was conducted utilizing powder X-ray diffraction data and the respective diffractogram along with corresponding planes is depicted in Fig. 3. The XRD profile of synthesized TSP matched very well with the standard ICDD reference (card no. 04-011-3010). Such observation confirmed the phase of the synthesized product as calcium phosphate-based TSP. The matched 2θ positions and the planes of the sample are 7.52 (010), 15.16 (020), 15.70 (001), 18.16 (011), 22.96 (021), 24.17 (−120), 26.66 (−1−31), 28.39 (−102), 30.32 (−112), 30.509 (040), 32.84 (0−41), 33.62 (0−22), 34.76 (140), 36.63 (022), 37.63 (131), 45.46 (1−22), 46.80 (211), 51.00 (−312), 54.21 (−303), 59.94 (202). Since all the visualized reflections were in line with the mentioned standard of TSP and no 2nd phase was logged, these results were good evidence supporting the formation of a single phase of TSP. Different crystallographic parameters such as crystallite size, lattice parameters, dislocation density, microstrain, and crystallinity index were estimated employing eqn (6)–(9), the details of these equations being explained in previous literature.[20,25] The TSP crystals are triclinic crystals of the $P\bar{1}(2)$ space group. This phosphate-based fertilizer is also known as hydrogen calcium phosphate hydrate with a molecular weight of 252.06 g mol^{-1}.

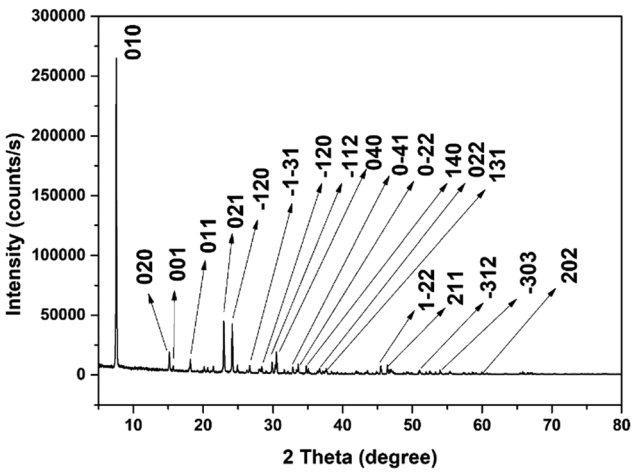

Fig. 3 X-ray diffraction pattern of TSP.

$$\text{Crystallite size, } D_c = \frac{K\lambda}{\beta\cos\theta} \quad (6)$$

$$\text{Dislocation density, } \delta = \frac{1}{(D_c)^2} \quad (7)$$

$$\text{Microstrain, } \varepsilon = \frac{\beta}{4\tan\theta} \quad (8)$$

$$\text{Crystallinity index, } CI = \frac{H_{(010)} + H_{(021)} + H_{(-120)}}{H_{(010)}} \quad (9)$$

In eqn (6), K is the Scherrer constant (0.94); β is full width at half maximum (FWHM, in radians); λ is wavelength of the Cu X-ray source; and θ is diffraction angle. The notation $H_{(hkl)}$ in eqn (9) represents peak height of (hkl) plane or respective plane.

The crystallite size, dislocation density, microstrain and crystallinity index calculated using eqn (6)–(9) were 100 nm, 0.00011 line per m^2, 0.0052, and 1.39, respectively. In this case line dislocation of the synthesized product was considered.

The preference of the crystal plane in the case of growth during the reaction within the prescribed experimental conditions is another vital parameter for crystallographic characterization of materials and this phenomenon can be expressed as preference growth. The preference growth can be estimated by comparing the relative intensity (RI) of one plane to the other three strong planes. In the case of TSP, the RI of (010) plane was calculated with respect to (021), (−120) and (020) planes. Thus, in this case the RI along (010) plane was compared with the RI of (021), (−120) and (020) planes which was estimated using eqn (10).[20] To compute the preference growth of a plane, the value of RI of the standard sample is also essential and in this case ICDD card no. 04-011-3010 was taken into account.

$$\text{Relative intensity, } RI_{gypsum} = \frac{I_{(010)}}{I_{(021)} + I_{(-120)} + I_{(020)}} \quad (10)$$

Here, the subscript of the intensity denotes the plane associated with the intensity. The relative intensity values of TSP sample and the standard were 1.5989 and 0.5899, respectively.

The preference growth of the sample was calculated using eqn (11) for TSP.[26]

$$\text{Preference growth, } P = \frac{\text{Relative intensity of sample} - \text{Relative intensity of standard}}{\text{Relative intensity of standard}} \quad (11)$$

Calculated preference growth of the (010) plane was 1.71 with respect to (021), (−120), and (020) planes while the preference growth of (021) plane against (010), (−120), and (020) planes was −0.50. In a similar fashion, the values calculated for (020) and (−120) planes were 1.06 and −0.58, respectively. These values clearly indicated that the preference growth along (010) plane was more favored or thermodynamically favorable than that along the other three planes under the present reaction conditions. Two negative signs indicated less preference for the plane during the formation of TSP within the set reaction parameters.

The specific surface area of TSP was measured from the crystallite size as well as the density (ρ) according to eqn (12).[27] The crystallite size was taken from that measured from the Scherrer equation and the value of density was found in the ICDD database. The computed value of specific surface area for TSP was 27 $m^2\ g^{-1}$.

$$\text{Specific surface area, } S = \frac{6 \times 10^3}{\rho \times D_c} \quad (12)$$

Crystallite size calculation using various models

Sahadat–Scherrer model. Crystallite size of any crystalline material is of considerable importance in the context of synthesis to application. To estimate the crystallite size properly, a number of model equations have been employed. The Sahadat–Scherrer model is a modified version of the Scherrer model which includes all the generated reflections to get a more precise crystallite size in the case of powder diffraction. The details of this model are explained elsewhere and the mathematical representation of the model is expressed in eqn (13).[20,28]

$$\text{Sahadat} - \text{Scherrer model: } \cos(\theta) = \frac{K\lambda}{D_{S-S}} \times \frac{1}{\text{FWHM}} \quad (13)$$

Fig. 4 presents the relevant graph generated from the Sahadat–Scherrer model and the crystallite size measured from this model was 99 nm.

Liner straight-line method of Scherrer equation. This model was also used to calculate crystallite size and a large value of crystallite size (1386 nm) was obtained from this model which suggests its inappropriateness for analysis. However, details of this model are described in ESI.†

Three peaks model. The Scherrer equation was used to estimate the crystallite size employing the average for three planes. For TSP the (010), (020) and (120) planes were considered to evaluate the crystallite size. Mathematically the ESI,† eqn (S_2)–(S_5) explain the three peaks model and the details can be found in the literature.[28] The crystallite size measured from this model was 88 nm for TSP which was close to that calculated from the Sahadat–Scherrer model.

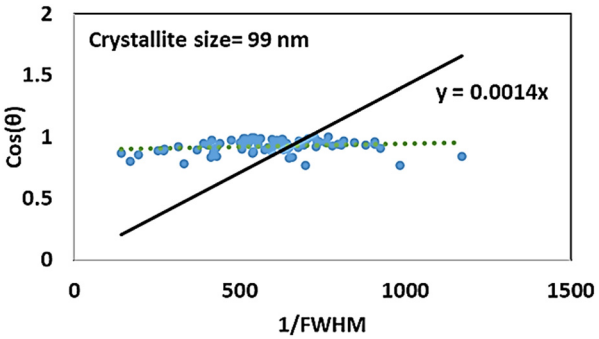

Fig. 4 Crystallite size estimation utilizing the Sahadat–Scherrer model.

Monshi–Scherrer model. The Monshi–Scherrer model is another format of the modified Scherrer model and was utilized to measure the crystallite size where a logarithm was considered on both sides. The details of the Monshi–Scherrer model can be found in the literature and can be expressed as eqn (S_6) (ESI†).[20,29] ESI,† Fig. S_2 presents the required graph for the TSP fertilizer and the computed crystallite size was 49 nm.

Williamson–Hall plot. The previously described models only consider the peak broadening from the crystals, but the Williamson–Hall model includes the instrumental broadening as well as broadening due to intrinsic strain. The crystallite size from the Scherrer equation depends on $1/\cos\theta$ but the Williamson–Hall plot is based on tan θ which allows the separation of peak broadening due to the crystallite size as well as microstrain.[30] The mathematical expression of the Williamson–Hall plot can be written as in ESI,† eqn (S_7)–(S_9), and the details of these equations are described elsewhere.[30,31] The crystallite size and microstrain of TSP were 99 nm and 0.0002, respectively, which were calculated from the uniform deformation model (the corresponding graph is presented in ESI,† Fig. S_3). The Young's modulus of TSP was reported as 45 GPa in the literature.[32] The USDM provided a crystallite size of 99 nm and stress of 0.0099 GPa in the case of TSP, and the constructed graph is documented in ESI,† Fig. S_4. The same crystallite size was noted for the uniform energy density deformation model and the energy density was 1.1×10^{-5} kJ m^{-2} (pictorial view is presented in ESI,† Fig. S_5).

Particle size and zeta potential analysis

The particle size of the synthesized products was analyzed using the DLS method, the results of which are presented in Fig. 5. The average particle size was estimated to be 740 nm which was very much larger than the crystallite size measured from the XRD technique. In the DLS method, the sample was dispersed in ethanol solution as TSP is completely soluble in water medium. The observed diameter was the hydrodynamic volume of the particle and thus a higher value was found. The measured zeta potential was 44 mV in ethanol solution which indicated a stable phase in ethanol solution.

Functional group analyses

FT-IR investigation. The functional groups of the synthesized TSP [$Ca(H_2PO_4)_2{\cdot}(H_2O)$] were explored using FT-IR

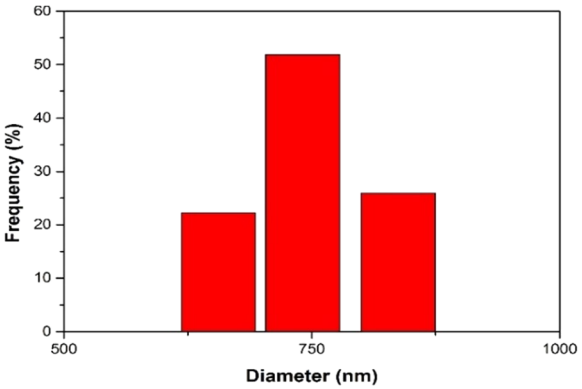

Fig. 5 Particle size analysis using the DLS method.

spectroscopy. In the composition of TSP Ca-oxide, –OH, and PO_4^{3-} groups are present which give peaks in the IR spectrum. The bending vibrations of O–P–O groups were noticed in the wavenumber range 450–600 cm^{-1} while the peaks due to stretching vibration were in the region of 900–1100 cm^{-1}. The in-plane and out-of-plane vibrations of P–O bonds were visualized near 1200–1250 and 800–900 cm^{-1} respectively. Bending and stretching modes of water molecules appeared near the regions of 800, 2800, 3200, and 3500 cm^{-1}. A similar type of spectrum was reported in the literature.[33] Fig. 6 presents the FT-IR spectrum of TSP synthesized from *P. globosa*.

Raman analysis. Raman-active groups were identified from the spectrum of Raman shift which is shown in ESI,† Fig. S_6. The difference between the FT-IR and Raman spectra is in the symmetry of the compound which originates mainly from the polarity of atoms or groups of atoms. Similar to the FT-IR spectrum, the Raman shift attributed to the bending vibration of O–P–O also appeared in the region of 450–600 cm^{-1}. In the Raman spectrum peaks appeared in the regions of 420, 480, 540, 567, 675, and 850 cm^{-1} and very similar peaks were observed in the FT-IR spectrum. However, overlapping among the peaks of the phosphate group was observed which could be due to the dissimilarity of vibration modes.

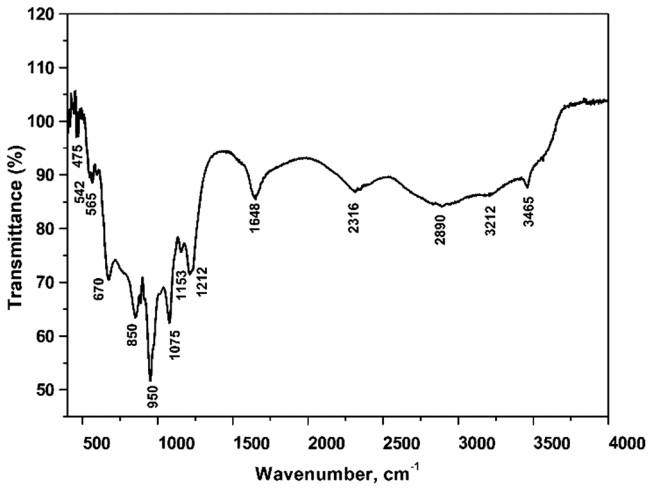

Fig. 6 FT-IR spectrum of TSP synthesized from *P. globosa*.

Field emission scanning electronic microscopic analysis

Fig. 7 visualizes the morphology of TSP synthesized from *P. globosa*. The image shows the sheet-like structure of the synthesized TSP with irregularity of the size and shape and a few rod-shape particles were also noticed. The particle sizes of TSP were not uniform and the particles remained in an aggregated state. The calculation of preference growth revealed that two planes of crystals were thermodynamically favored by the reaction conditions and another plane exerted unstable growth carrying negative value. The pictorial view of TSP supported the data for the growth preference of two directions.

Optical bandgap estimation

To calculate the optical bandgap, the Tauc plot was used and the mathematical expression of the technique can be represented as eqn (14).[34,35] The bandgap energy of any material is a very crucial parameter to characterize the material in terms of photochemical as well as photophysical properties as it explains the electronic transition of valence band to conduction band.[36] There are four types of optical bandgap, namely direct allowed ($n = 1/2$), direct forbidden ($n = 3/2$), indirect allowed ($n = 2$) and indirect forbidden ($n = 3$);[37] however, in this case only direct allowed bandgap was estimated as shown in Fig. 8. The transmittance/reflectance properties of TSP were explored from UV-Vis-NIR data and the calculated value from the Tauc plot was 3.84 eV.

$$\propto h\nu = A(h\nu - E_g)^n \quad (14)$$

Wavelength-dispersive X-ray fluorescence

To measure the chemical compositions of the synthesized products, WDXRF analysis was performed. The percentages of P_2O_5 and CaO are the quality-determining factors of TSP fertilizer. The raw *P. globosa* shells contained CaO (97.0%), SiO_2 (0.735), MgO (0.17%), Fe_2O_3 (700 ppm), Al_2O_3 (0.53%), and other negligible metal oxides. The synthesized TSP contained P_2O_5 (76.9%), CaO (22.6%), SiO_2 (0.11), MgO (914 ppm), Fe_2O_3 (907 ppm), Al_2O_3 (529 ppm), ZnO (293 ppm), and other negligible metal oxides. Commercial fertilizer is supposed to comprise 46% P_2O_5 for the application of phosphate-based fertilizer.[38,39] A higher percentage of P_2O_5 content will definitely

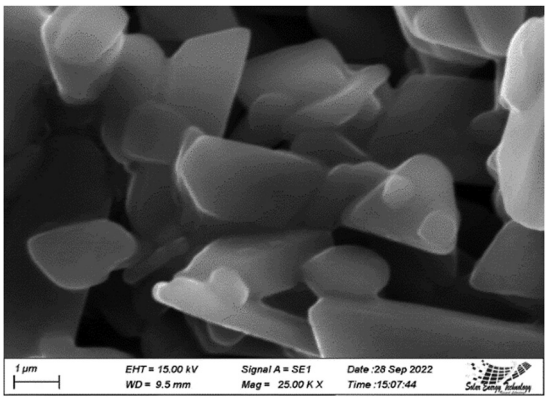

Fig. 7 SEM image of TSP synthesized from *P. globosa*.

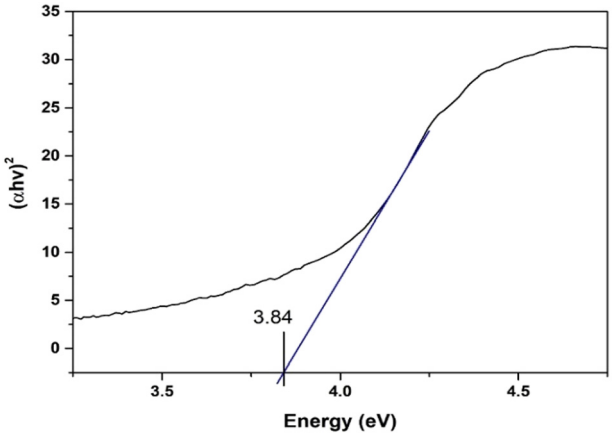

Fig. 8 Estimation of optical bandgap energy of synthesized TSP.

improve the applicability of the synthesized fertilizer. The TSP contained Zn which is also another micronutrient for the growth of plants.[40] Iron and magnesium are also useful in plant growth which are also contained in the TSP synthesized from waste *P. globosa* shells.[41] Researchers found that plants can accumulate heavy metals in the roots and body which are absorbed from the soil.[42] In the reported synthesized TSP, no heavy metals were found in WDXRF analysis; thus no risk related to heavy metals can originate from using this fertilizer in the field. Use of fertilizer with some metal impurities is reported in the literature.[43]

Moisture content

The moisture content of TSP was measured to report the safe storage facilities and a temperature variation was maintained for the accuracy of the technique. The moisture content of TSP at 120 °C was 5.41%. It was measured using a moisture analyzer instrument. Whereas the TGA data revealed nearly 3% mass was lost at 120 °C which was reached within 10 min. The difference in the lost mass may be due to the duration of the sample remaining. Though a commercial instrument was utilized to estimate the moisture content, to provide better storage facility the 120 °C temperature is too high to get any prediction. Therefore, a lower temperature such as 50 °C was chosen maintaining 500 mmHg pressure for 2 h which revealed the moisture content to be 3.23%.

Conclusion

TSP was successfully synthesized from waste *P. globosa* shells for industrial sustainability using a waste recycling procedure. The synthesized TSP was confirmed by a number of analytical techniques and no abnormality or difficulty was experienced during the synthesis process. The data also revealed that no extra drying procedure is necessary if 60% (w/w) phosphoric acid can be chosen as the source of phosphate, where more than 98% yield can be achieved. The TGA and DSC data articulated the thermal behavior indicating water removing ranges that may be considered during drying of conventional P-fertilizer produced in industry. Indeed, TGA showed promising results by providing the remaining mass (including 2.42% free water) value as 77.63%, which is very close to the theoretical remaining mass percentage (78.57%). Thus, this observation confirms the formation of TSP in nearly pure phase. From this research it is suggested to consider *P. globosa* shells as a precursor of calcium as a new raw material source of P-fertilizer and 60% (w/w) phosphoric acid to minimize the production cost by eliminating the extra drying process with 76.9% P_2O_5 content.

Data availability

The raw/processed data required to reproduce these findings cannot be shared at this time due to technical or time limitations.

Author contributions

Md. Sahadat Hossain conceived and designed the experiment, analysed the data, wrote the original manuscript and performed the experiment. Md. Aftab Ali Shaikh supervised the overall work and managed the funding with required facilities. Md. Farid Ahmed executed the particle size and zeta potential analysis. Samina Ahmed supervised the overall work and managed the funding with required facilities.

Conflicts of interest

There are no conflicts to declare.

Acknowledgements

The authors are grateful to Bangladesh Council of Scientific and Industrial Research (BCSIR) authority for financial support through R&D project (ref. no. 39.02.0000.011.14.134.2021/900; date: 30.12.2021). The authors also thank Dr Shirin Akter Jahan, Project Director of Strengthening of IGCRT for instrumental support. The authors are also grateful to Sabrina Mostofa, Senior Scientific Officer for executing the WDXRF analysis.

References

1 S. Mauro da Silva Neiro, É. V. de Faria and V. V. Murata, *Ind. Eng. Chem. Res.*, 2022, **61**, 4031–4045.
2 L. Jordan-Meille, G. H. Rubæk, P. A. I. Ehlert, V. Genot, G. Hofman, K. Goulding, J. Recknagel, G. Provolo and P. Barraclough, *Soil Use Manage.*, 2012, **28**, 419–435.
3 D. Cordell, J.-O. Drangert and S. White, *Glob. Environ. Change*, 2009, **19**, 292–305.
4 W. M. Stewart, L. L. Hammond and S. J. Van Kauwenbergh, *Phosphorus: agriculture and the environment*, 2005, vol. 46, pp.1–22.
5 T. Zou, X. Zhang and E. A. Davidson, *Nature*, 2022, 1–7.
6 D. M. R. Sekhar, M. K. Katewa and M. S. Shaktawat, *Nat. Preced.*, 2012, 1.
7 D. Cordell and S. White, *Annu. Rev. Environ. Resour.*, 2014, **39**, 161–188.

8 T. Worstall, *Nature*, 2013, **493**, 163.
9 J. Liu, A. Balmford and K. S. Bawa, *Nature*, 2022, **604**, 425.
10 Z. Huang, S. Zhang, H. Wang, R. Liu, C. Cheng, Z. Liu, Z. Guo, X. Yu, G. He and G. Ai, *J. Agric. Food Chem.*, 2020, **68**, 11114–11120.
11 J. D. Hatfield, D. W. Rindt and A. V. Slack, *Ind. Eng. Chem.*, 1959, **51**, 677–682.
12 K. Nasri, H. El Feki, P. Sharrock, M. Fiallo and A. Nzihou, *Ind. Eng. Chem. Res.*, 2015, **54**, 8043–8047.
13 B. F. Mohazzab, B. Jaleh, M. Nasrollahzadeh, S. Khazalpour, M. Sajjadi and R. S. Varma, *ACS Omega*, 2020, **5**, 5888–5899.
14 G. Ashrafi, M. Nasrollahzadeh, B. Jaleh, M. Sajjadi and H. Ghafuri, *Adv. Colloid Interface Sci.*, 2022, 102599.
15 Y. Orooji, N. Han, Z. Nezafat, N. Shafiei, Z. Shen, M. Nasrollahzadeh, H. Karimi-Maleh, R. Luque, A. Bokhari and J. J. Klemeš, *J. Cleaner Prod.*, 2022, 131220.
16 M. Nasrollahzadeh, N. S. Soheili Bidgoli, N. Shafiei, F. Soleimani, Z. Nezafat and R. Luque, *Biofuels, Bioprod. Biorefin.*, 2020, **14**, 1197–1227.
17 C. Xu, M. Nasrollahzadeh, M. Selva, Z. Issaabadi and R. Luque, *Chem. Soc. Rev.*, 2019, **48**, 4791–4822.
18 S. Parveen, A. Chakraborty, D. K. Chanda, S. Pramanik, A. Barik and G. Aditya, *ACS Omega*, 2020, **5**, 25757–25771.
19 D. Madhu, R. Arora, S. Sahani, V. Singh and Y. C. Sharma, *J. Agric. Food Chem.*, 2017, **65**, 2100–2109.
20 M. S. Hossain and S. Ahmed, *RSC Adv.*, 2022, **12**, 25096–25105.
21 J. A. Barreiro Jr, A. Minichini, J. A. Barreiro and A. J. Sandoval, *Ind. Eng. Chem. Res.*, 2010, **49**, 887–892.
22 A. E. Newkirk, *Anal. Chem.*, 1960, **32**, 1558–1563.
23 P. Wang, M. Wei, Y. Dong, Z. Zhu, J. Liu, J. Pang, X. Li and J. Zhang, *J. Non-Cryst. Solids*, 2022, **594**, 121824.
24 O. Toshev, T. Safronova, M. Kaimonov, T. Shatalova, E. Klimashina, Y. Lukina, K. Malyutin and S. Sivkov, *Ceramics*, 2022, **5**, 516–532.
25 Y. Fu, M. T. Rea, J. Chen, D. J. Morrow, M. P. Hautzinger, Y. Zhao, D. Pan, L. H. Manger, J. C. Wright and R. H. Goldsmithss, *Chem. Mater.*, 2017, **29**, 8385–8394.
26 M. S. Hossain, M. A. A. Shaikh, M. S. Rahaman and S. Ahmed, *Mol. Syst. Des. Eng.*, 2022, **7**, 1239–1248.
27 K. V. Kumar, T. J. Subha, K. G. Ahila, B. Ravindran, S. W. Chang, A. H. Mahmoud, O. B. Mohammed and M. A. Rathi, *Saudi J. Biol. Sci.*, 2021, **28**, 840–846.
28 Md. S. Hossain, M. Mahmud, M. B. Mobarak, S. Sultana, Md. A. A. Shaikh and S. Ahmed, *Chem. Pap.*, 2022, **76**, 7245–7251.
29 M. A. Islam, A. K. M. Akther Hossain, M. Z. Ahsan, M. A. A. Bally, M. Samir Ullah, S. M. Hoque and F. A. Khan, *RSC Adv.*, 2022, **12**, 8502–8519.
30 D. Jamwal, G. Kaur, P. Raizada, P. Singh, D. Pathak and P. Thakur, *J. Phys. Chem. C*, 2015, **119**, 5062–5073.
31 A. Velazquez-Palenzuela, F. Centellas, J. A. Garrido, C. Arias, R. Maria Rodriguez, E. Brillas and P.-L. Cabot, *J. Phys. Chem. C*, 2010, **114**, 4399–4407.
32 S. Seesanong, C. Seangarun, B. Boonchom, C. Sronsri, N. Laohavisuti, K. Chaiseeda and W. Boonmee, *Minerals*, 2022, **12**, 254.
33 S. Seesanong, C. Seangarun, B. Boonchom, N. Laohavisuti, K. Chaiseeda and W. Boonmee, *ACS Omega*, 2021, **6**, 22065–22072.
34 M. Nazim, A. A. P. Khan, A. M. Asiri and J. H. Kim, *ACS Omega*, 2021, **6**, 2601–2612.
35 S. K. Suram, P. F. Newhouse and J. M. Gregoire, *ACS Comb. Sci.*, 2016, **18**, 673–681.
36 P. Makula, M. Pacia and W. Macyk, *J. Phys. Chem. Lett.*, 2018, **9**, 6814–6817.
37 D. Sidorczuk, M. Kozanecki, B. Civalleri, K. Pernal and J. Prywer, *J. Phys. Chem. A*, 2020, **124**, 8668–8678.
38 Triple Super Phosphate Fertilizer, **https://yuyuangroup.en.made-in-china.com/product/BXKJdScCPbpv/China-Triple-Super-Phosphate-Fertilizer.html**, (accessed October 18, 2022).
39 J. H. Falls, *Fert. Res.*, 1991, **28**, 239–249.
40 S. K. Ray, C. Varadachari and K. Ghosh, *Ind. Eng. Chem. Res.*, 1993, **32**, 1218–1227.
41 I. Bhattacharya, S. Bandyopadhyay, C. Varadachari and K. Ghosh, *Ind. Eng. Chem. Res.*, 2007, **46**, 2870–2876.
42 P. N. Kumar, V. Dushenkov, H. Motto and I. Raskin, *Environ. Sci. Technol.*, 1995, **29**, 1232–1238.
43 M. Gargouri, C. Chtara, P. Charrock, A. Nzihou and H. El Feki, *Ind. Eng. Chem. Res.*, 2011, **50**, 6580–6584.